1
2
3
4
5
6

Unexpected Early Proteomic Changes in Alzheimer's Disease Model Mice Synaptosomes

9
10
11
12
13
14

15 Kerri Ball[1], Addolorata Pisconti[1], Kelly Grounds[1], William M. Old[1,*], Michael
16 H. B. Stowell[1,2,*]

17
18
19
20
21

22 [1]The Department of Molecular, Cellular, and Developmental Biology, University of
23 Colorado, Boulder, Colorado 80309-0347

24 [2]The Department of Mechanical Engineering, University of Colorado, Boulder, Colorado
25 80309-0347

26

28

29 *To whom correspondence should be addressed. E: william.old@colorado.edu,
30 E:stowellm@colorado.edu

1

Abstract

31

32   We have employed label-free quantitative proteomics of wild-type and Alzheimer's

33   disease (AD) model mice synaptosomes to investigate proteomic changes occurring

34   during AD progression as a prelude to analysis in humans. More than 4000 proteins were

35   analyzed using multiple analysis tools and statistical criteria. Pathway enrichment

36   identified numerous pathways consistent with the current AD knowledge base, including

37   dysregulation of Glutamate Receptor Signaling, Synaptic Long Term Potentiation and

38   Depression, Rho and Rac Signaling, Calcium Signaling, and Oxidative Phosphorylation

39   and Mitochondrial Dysfunction. Additionally, the data demonstrate that a large number of

40   changes occur in the proteome very early relative to the onset of both traditional disease

41   markers such as amyloid accumulation, tau phosphorylation and cognitive dysfunction.

42   These early changes include a number of dysregulated proteins that have novel

43   associations with AD progression. These results reinforce the importance of mechanistic

44   investigations in early disease progression long before the classical markers of

45   Alzheimer's disease are observed.

Introduction

47   The synapse is the localized contact between nerve cells required for signal

48   transmission and AD is considered by many to be a synaptic disease. This cell-to-cell

49   communication is characterized by complex protein-driven molecular mechanisms

50   including synthesis, delivery, storage, docking, fusion, neurotransmitter release and

51   reuptake (1). Synapses can be studied by isolation of synaptosomes which contain the

52   complete presynaptic terminal, including mitochondria and synaptic vesicles, along with

53 the postsynaptic membrane and the postsynaptic density. Several proteomic studies of

54 synaptosomes have previously been performed (2–5). However, only recently has mass

55 spectrometric analysis reached the level of technical advancement necessary for a direct

56 and comprehensive analysis of the synaptic proteome (6). These advances in proteomics

57 technologies allow direct and unbiased examination of protein level differences in

58 neurodegenerative diseases and have great potential to shed new light on disease

59 pathogenesis. Here, we employed these technical advancements in mass spectrometry

60 for the detection of more than 4,000 synaptosomal proteins using label-free quantitative

61 proteomics to characterize the proteome changes that occur in Alzheimer's disease (AD)

62 model mice. Multiple structural and/or metabolic proteins have been reported to have

63 altered expression in AD supporting a high depth quantitative proteomic analysis for

64 target discovery (7–10).

65

66 # Results

67 ## Mouse Model Characterization

68 The B6C3-Tg(APPswe,PSEN1dE9)85Dbo/Mmjax mouse model (Tg-AD) of

69 Alzheimer's disease is a widely used model for AD; it contains a chimeric mouse/human

70 amyloid precursor protein (APP)(Mo/HuAPP695swe) and human presenilin 1 (PS1-dE9);

71 both driven by the prion protein promoter and therefore expressed in central nervous

72 system neurons (11–15). These two insertions favor processing through the β-secretase

73 pathway and, thus, elevate the amount of amyloid-beta (Aβ) fragments produced from the

74 APP transgene. To validate accumulation of Aβ fragments in transgenic mice, we used

3

75   commercially available ELISA kits specific for Aβ 1-42. As shown in Fig1, both Aβ 1-42

76   accumulates in the brain of Tg-AD mice in an age dependent manner, supporting the

77   choice of this mouse strain as a relevant model of AD.

78   **Fig1. Amyloid accumulation in the APPswe/PSEN1dE9 Alzheimer's disease**

79   **mouse model.** (A.) Human Aβ42 was quantitated using commercially available

80   sandwich ELISA kits at the indicated ages using both wild-type (WT) and Tg-AD

81   (B6C3-Tg (APPswe, PSEN1dE9)85Dbo/J)) mice. Amounts of Aβ42 were

82   normalized to total protein as determined by BCA Assay. (B.) Three, five and nine

83   month old Tg-AD mice were chosen for high depth proteomic analysis based on

84   the stages of Aβ load, plaque development, and cognitive decline.

85   Based on our Aβ accumulation data (Fig1) and upon previous characterizations of

86   the APPswe, PSEN1dE9 biogenic mouse model which describe the timing of cognitive

87   impairment and plaque formation (11–15), we chose to carry out a proteomic analysis of

88   the synaptosomes of three, five, and nine month-old mice. These three age groups

89   represent three distinct stages of AD, summarized in Fig1C. The three month-old Tg-AD

90   age group have minimal accumulation of Aβ1-42, normal cognitive function, and complete

91   absence of plaques. The five month-old Tg-AD mice have relatively high levels of Aβ1-42

92   which are accompanied by the presence of sporadic plaques although no cognitive

93   decline has been reported. In contrast, the nine month-old Tg-AD mice represent the post-

94   plaque and post-cognitive decline stage of AD.

4

95

Workflow

97   Synaptosomes from 3, 5, and 9 month-old Tg-AD and wild-type (WT) mice were

98 isolated according to standard protocols (16). Filter Assisted Protein Preparation (FASP)

99 was utilized to obtain pure peptides for LC-MS/MS analysis (17). Peptide samples were

100 analyzed by online two dimensional reverse phase (RP/RP) nanoflow HPLC-MS/MS.

101 Raw mass spectrometry data was converted to protein abundance using chromatography

102 feature finding software MaxQuant (version 1.5.2.8) (18–20).

103   A total of 4,655 proteins were identified across all 18 samples using MaxQuant

104 (18–20). All proteins categorized as potential contaminants, reverse sequence, and/or

105 only identified by site were removed from the analysis. Biological replicates were than

106 categorically annotated into 6 groups and proteins containing less than 2 valid values in

107 each group were removed from the analysis, thus reducing the matrix to 3312 quantifiable

108 proteins. (S1 Data File).

109   **S1 Data File. Protein Quantification and Analysis.**

110

Qualitative Analysis

112   A qualitative evaluation of the MS data was performed on both the WT and AD

113 data. While biological variation is expected and accepted among replicates, due to

114 complex and step-wise collection of RP/RP HPLC MS/MS data technical variations

115 should be evaluated. For this analysis, we started with a hierarchical cluster analysis

116   (HCA) performed using complete-linkage clustering with Euclidean distance metrics of

117   the nine WT samples (Fig2A) and the nine AD samples (Fig2B). As shown in Fig2A, the

118   sample WT_3M_12f-C was identified as a potential outlier to other eight WT samples that

119   are all merged into one cluster. The sub-clusters of the eight WT samples include pair-

120   wise clustering of 3M with 5M and 5M with 9M, suggesting that age-dependent difference

121   between the three WT age groups are negligible. In contrast, the main 2 clusters in the

122   AD HCA (Fig2B) have a relatively short distance between them and the sub-clustering

123   pairs include age matched AD samples, such as the pairing of AD_3M_14c-F with

124   AD_3M_12f-AD, AD_9M_16c-CF with AD_9M_16a-D, and AD_5M_11a-C with

125   AD_5M_11a-AB. Thus, the AD HCA suggests that differences between the age groups

126   and, moreover, differences between the three selected stages of Alzheimer's disease will

127   be observed.

128   **Fig2. Qualitative Assessment of MS/MS data.** A dendogram of the WT samples

129   (A.) and the AD samples (B.) produced using Euclidean distance with complete

130   linkage of LFQ intensity data with all invalid values removed. (B.) Histogram of

131   absolute $\log_2$ expression values (ORANGE: WT_x – WT_average =, GREEN:

132   3M_x – 3M_average, BLUE: 5M_x – 5M_average, YELLOW: 9M_x –

133   9M_average).

134

135   To further explore the variability between replicates, we evaluated the $\log_2$ fold

136   change of individual samples from the average (Fig2C, ORANGE: WT from the average

137   WT, GREEN: 3M_AD from the average 3m Tg-AD, BLUE: 5M_AD from the average 5m

138   Tg-AD, and YELLOW: 9M_AD from the average 9m Tg-AD). The expectation is that all

6

139 samples included in the average should have a similar shaped distribution, thus the

140 shorter and broader shape of the sample WT_3M_12f-C distribution compared to the

141 other WT samples further supports the identification of this sample as an outlier. The

142 3M_AD samples all have a similar distribution, despite the Euclidean distance of sample

143 AD_3M_14c-A from the other two 3M_AD samples (Fig2B). While the AD_5M and

144 AD_9M sample distributions are a clear reflection the short Euclidean distances observed

145 in Fig2B; in particular, the distance between AD_5M_11a-C and AD_5M_11a-AB is

146 shorter than for any other pairing and the distribution of these samples is taller and more

147 narrow than any of the other samples.

148   Together, this qualitative evaluation of the MS/MS data identifies sample

149 WT_3M_12f-C as an outlier that will be excluded from the quantitative analysis.

150 Additionally, this analysis supports that age dependent biological variability between the

151 control groups is very small. Grouping the 8 WT samples in one control group increases

152 the statistical power of the analysis, but may sacrifice age specific variations, thus further

153 evaluation of age dependent protein abundance was analyzed.

154   To determine if pooling the WT samples would be appropriate, we analyzed

155 potential age-dependent changes in the WT samples using an ANOVA multi-sample test.

156 No statistically significant proteins were identified using a loose False Discover Filter

157 (FDR, Bengamini-Hochburg) α = 0.25. Thus, to identify genes that would likely lose

158 statistical relevance if an average WT was used rather than age matched controls, we

159 applied a p-Value cut-off of 0.1 with no FDR and an absolute $\log_2$ fold change filter of 0.5.

160 We identified 73 proteins of interest (S1 Data File) that could be lost if we pooled the WT

161   samples into a single control group. However, despite these potential loses, we made the

162   decision to group all of the WT samples into a single control group.

163

Quantitative Assessment of Alzheimer's Disease Progression Proteome

165   R-limma (21–23) was used to perform a quantitative assessment of proteome

166   differences between the following groups: 3m Tg-AD & WT, 5m Tg-AD & WT, and 9m Tg-

167   AD & WT. Empirical Bayes statistics was used to calculate p-Values. Using a Bengamini-

168   Hochburg FDR α = 0.1, (Fig3; S1 Data File). Surprisingly, the majority of statistically

169   significant proteins identified were only significant in the pre-plaque, 3m Tg-AD, stage of

170   AD when $A\beta$ levels are still very low. The protein expression profiles of the top most

171   dysregulated proteins ($\log_2$ FC >= |1|) are shown in Fig4. We noted that even though the

172   selection of significant proteins was dominated by the 3m Tg-AD statistical analysis, clear

173   age dependent data trends were observed; we clustered the proteins based on these

174   expression trends. This clustering shows groups of proteins that decrease (clusters 2 &

175   3) and increase (clusters 8, 9, & 10) during AD progression, that are consistently up

176   (cluster 1 & 2) or down (cluster 10 & 11), and that have stage specific protein

177   dysregulation (clusters 4, 5, 6, & 7). Eleven of the proteins of interest identified have a

178   previous association with $A\beta$ and/or AD (Fig4 *GENE), while 73 of these high confidence

179   proteins ($\log_2$ FC >= |1|) are novel to our understanding of AD progression.

180   **Fig3. Quantitative Analysis of Age-Dependent Alzheimer's Disease.** R-limma

181   was used to calculate the p-Value and $\log_2$ fold change for the 3312 quantifiable

182   proteins using the following groupings: (A.) 3m Tg-AD & WT, (B.) 5m Tg-AD & WT,

183   and (C.) 9m Tg-AD & WT. A Bengamini-Hochburg FDR α = 0.1 is indicated with a

184   solid line in each graph and the significant proteins are colored. This data and the

185   corresponding gene names are included in Supplement File 1.

186

187   **Fig4. High-Confidence Protein Expression Profiles and Clusters.** Proteins

188   were filtered using an FDR = 0.1 and an absolute FC = 1 in at least one age group.

189   Proteins were clustered based on observable FC trend. Proteins with a previously

190   recognized association with Aβ (24) and/or recognized by Kegg as "Alzheimer's

191   Disease: are indicated by * next to the gene name.

192

STEM Analysis

193

194   As mentioned above, we observed many proteins that appeared to have a linear

195   trend of protein expression. Time-dependent data trends can further increase confidence

196   in the data, and analysis of these trends may even identify addition statistically significant

197   protein changes. To further explore proteins with trending protein profiles we utilized the

198   Short Time-series Expression Miner (STEM)(25). We used a maximum of 50 model

199   profiles and maximum unit change of 3 (log$_2$ FC) between time points to profile the matrix

200   of 3312 quantifiable proteins at the three Tg-AD age groups. STEM profile enrichment

201   identified 121 proteins that follow one of five significant profiles (S2 Data File). Fig5A-E

202   shows these significant STEM profiles (black); the protein expression patterns that were

203   fitted to these profiles are plotted along with the STEM profiles. Not quite half the proteins

204   identified by STEM (58/121 proteins) were identified as significant using the empirical

205   Bayes statistical enrichment, while 63 new proteins were added to the list of proteins

206   dysregulated during the progression of AD.

207   **S2 Data File. Time-series expression analysis by STEM.**

208   **Fig5. Significant Protein Trends identified by STEM.** Five protein expression

209   profiles were identified as having more proteins fitting to the profile than would be

210   expected by random chance. These significant profiles included three increasing

211   profiles with 41 proteins fitting the -3, 0, 1 $\log_2$ FC profile (A.) in the 3m, 5m, and

212   9m age groups, respectively, 25 proteins fitting the -1, 0, 3 $\log_2$ FC profile (B.), and

213   16 proteins fitting the -2, -1, 1 $\log_2$ FC profile (C.). Two decreasing profiles were

214   also identified; these were characterized by 25 proteins fitting the 3, 0, -1 $\log_2$ FC

215   profile (D.) and 14 proteins fitting the 2, 1, -1 profile (E.) The profile summaries

216   exported from STEM can be found in S2 Data File and the protein-to-profile

217   assignments can be found in S2 Data File as well as in S1 Data File.

218

Canonical Pathway Enrichment

220   The benefit of adding proteins identified by STEM is demonstrated in Fig6 where

221   Canonical Pathway Enrichment (by Ingenuity Pathway Analysis, IPA) is compared

222   between three data filters for the 3m Tg-AD data set: a strict filter (FDR 0.1 + $\log_2$ FC >=

223 |1|), an FDR only filter (FDR 0.1), and a STEM enriched filtered data set (FDR 0.1 + $\log_2$

224   FC >= |0.4|, +STEM proteins) for a select group of canonical pathways (complete list: S3

225   Data File). P-values for canonical pathways are calculated in IPA using a right-tailed

226   Fisher Exact Test that considers the overlap of observed and predicted genes in a

10

227 pathway. Thus, while strict data filters will result in a high confidence gene list (Fig4), a

228 short gene list will also produce a low confidence canonical pathway enrichment.

229 Additionally, Fig6 & S3 Data File show that, with few exceptions, expanding the gene list

230 to include lower confidence protein expressions identified using STEM adds to our

231 pathway confidence (p-Value) or in other words, "what is significant becomes MORE

232 significant". IPA also assigns a Z-score that assesses the match of observed and

233 predicted up/down regulation patterns. Therefore, the age-dependent FC for all proteins

234 in the Canonical Pathway are considered. In IPA, a Z-score greater than 2 or less than -

235 2 is considered predictive; positive Z-scores indicate activation and negative Z-scores

236 indicate repression of the described function. As shown in Fig6, the STEM enriched

237 protein list allows higher confidence directional predictions in comparison the FDR only

238 filtered protein list. No predictable directionality was found in any of the enriched

239 Canonical Pathways when the high confidence protein list (FDR 0.1, |FC|>1) was used.

240 **S3 Data File. Canonical Pathway Enrichment.**

241 **Fig6. STEM proteins add confidence and direction to Canonical Pathway**

242 **Enrichment analysis.** Ingenuity Pathway Analysis (IPA) was used to analyze the

243 3m Tg-AD Canonical Pathway Enrichment using three different data filters: the

244 high confidence protein list from Fig4, a standard filter (FDR = 0.1 only), and the

245 STEM expanded FDR = 0.1 and absolute FC >= 0.4. p-Values and z-scores as

246 calculated by IPA are shown for the top Canonical Pathways. The complete

247 Canonical Pathway Enrichment list can be found in S3 Data File.

248

249   With this in mind we utilized the protein expression data from all proteins identified

250   as significant (FDR = 0.1, absolute $\log_2$ FC >= 0.4) plus the STEM identified proteins to

251   run a canonical pathway enrichment analysis. All pathways with a z-score in at least one

252   age group are shown in Fig7. Z-scores greater than or equal to the absolute value of two

253   are considered predictive. All dysregulated pathways, including those without a z-score,

254   can be found in S3 Data File.

255   **Fig7. Ingenuity Pathway Analysis (IPA) predicted direction of Canonical**

256   **Pathways.** IPA was used to analyze compare the directionality (z-scores) of

257   Canonical Pathways identified enriched in the STEM expanded FDR = 0.1 and

258   absolute FC >= 0.4 protein list. Canonical pathways with valid/non-zero z-score in

259   at least one age group are shown here. The complete Canonical Pathway

260   Enrichment list can be found in S3 Data File.

Discussion

262   The most well-known and well-studied histopathological hallmark of AD is an

263   increase in Aβ peptide abundance and subsequent formation of amyloid plaques.

264   Accordingly, the mouse model used in our studies should provide insights in downstream

265   mechanisms following Aβ production. Aβ is believed to be a crucial pathogenic factor in

266   AD development. Recent evidence indicates that the soluble-oligomeric forms of Aβ are

267   primarily responsible for the neurodegeneration and loss of synaptic function

268   characteristic of later stages of AD, and this soluble-Aβ hypothesis is further supported

269   by recent clinical data on aducanumab, a human monoclonal antibody shown to reduce

270   soluble and insoluble Aβ (26).

271   Surprisingly, we observed that the largest changes to the synaptosomal proteome

272   occurred in the 3m Tg-AD mouse model where Aβ levels are relatively low, Aβ plaques

273   are absent, and no cognitive decline is observable. While this is consistent with soluble-

274   oligomeric forms of Aβ being primarily responsible for the pathogenesis of AD, it is notable

275   that despite the large proteomic changes, the 3m Tg-AD mice have no observable

276   phenotype. Very recently, a new AD phenotype has been observed: olfactory recall

277   impairment occurs up to ten years prior to the onset of cognitive decline (27,28). This

278   suggests that the observed proteomic changes in the 3m Tg-AD mouse may have

279   correlated phenotypes that remain to be identified. However, it could also suggest that Aβ

280   has a significant biological impact on the brain, even at low levels, and that compensatory

281   mechanisms are not only active but, most importantly, are biological efficacious during

282   the preclinical stages of AD. Although the ultimate progression of AD suggests that any

283   early neuroprotective response to Aβ is not sustainable or is not sufficient to prevent

284   neurotoxicity.

285   In typical AD progression, Aβ promotes disturbances in a number of pathways that

286   ultimately lead to neurotoxicity. Specifically, Aβ oligomers have been reported to induce

287   NMDA receptor activation, mitochondrial Ca2+ overload/membrane depolarization,

288   oxidative stress and apoptotic cell death (29–32). Consistent with this pathology, we

289   observed dysregulation in these Canonical Pathways: Glutamate Receptor Signaling,

290   Synaptic Long Term Potentiation and Depression, Calcium Signaling, and Oxidative

291   Phosphorylation and Mitochondrial Dysfunction (Figures 6 & 7, S3 Data File). Beyond

292   observing dysregulation of Canonical Pathways that are consistent with what is already

293   known about AD, we identified 73 proteins with high confidence (log$_2$ FC >= |1|, Fig4) that

13

294   are novel in our understanding of AD progression, but that are consistent with previous

295   studies. While refraining from going through all proteins/pathways, a striking example of

296   how our data supports the existing knowledge can be found by close inspection of the

297   RhoA Pathway depicted in Fig8. Specifically, our data shows an increase RhoA GEF

298   protein (ARHGEF1) and a decrease in RhoA GAP protein (RHOGAP) in the 3m Tg-AD

299   (Fig8A), consistent with activation of RhoA Signaling Pathway (Fig8B). RhoA activation,

300   as shown in Fig8A & B, leads to the activation a number of kinases whose downstream

301   activities regulate the actin cytoskeleton. ROCK, for example, is a kinase downstream of

302   RhoA that activates LIMK which in turn phosphorylates, and thus inhibits, the actin

303   severing protein, cofilin (Fig8). However, in direct opposition to the IPA's predicted state

304   of cofilin, previous observations with Aβ1-42 treatment show an increase in

305   dephosphorylated cofilin (33) and an increase of cofilin translocation into the mitochondria

306   (consistent with dephosphorylated cofilin) (34). Moreover, in AD patients, a loss or

307   shortening of dendritic spines is observed, consistent with loss of cytoskeletal stability.

308   Previous studies have also shown that Aβ1-42 treatment of hippocampal neurons induced

309   increased activity in Rac1, Cdc42, and PAK1 (33), which, like RhoA, are also involved in

310   activation of LIMK and the phosphorylation of cofilin. Together, this data suggests that Aβ

311   either inhibits phosphorylation or promotes dephosphorylation of cofilin and that activation

312   of upstream activators of LIMK may be a compensation mechanism for the increase in

313   dephosphorylated cofilin. Potential mechanisms of Aβ's regulatory role on cofilin

314   phosphorylation and dephosphorylation are illustrated in Fig9A.

315   **Fig8. RhoA Signaling Pathway activation in early AD**. (A.) Canonical Pathway

316   enrichment analysis identified RhoA as activated in the 3m Tg-AD. (B.) The log$_2$

14

317   FC of eight proteins within the RhoA Signaling Pathway were used to calculate the

318   z-score and the predicted directionality of RhoA Signaling. (C.) These molecules

319   are colored red (up-regulated) or blue (down-regulated) in a schematic of the RhoA

320   Signaling pathway in the 3m Tg-AD. (D.) IPA's Molecular Activation Predictor

321   illustrates the predicted outcome of the 3m Tg-AD protein abundance changes.

322   (Red = activated; Blue = inhibited; Yellow = inconsistent with state of downstream

323   molecule)

324   **Fig9. Proposed Aβ's impact on Cofilin Phosphorylation and actin**

325   **stabilization.** Our study, in concert with previous studies, implicates Aβ

326   involvement in the activation of a number of molecules upstream of Cofilin

327   regulation and actin stabilization. (Red = activated; Blue = inhibited; Yellow =

328   inconsistent with state of downstream molecule)

329

330   Compensation for Aβ induced dysregulation of cofilin-actin dynamics would be

331   required for sustained neural function and survival. Cofilin-actin regulation is critical for

332   morphogenesis and the structural dynamics of neural spines and has been strongly

333   implicated in synaptic trafficking of AMPA receptors during Synaptic Potentiation and

334   Depression (35,36). In the 3m Tg-AD, we do not see a significant difference in the number

335   of AMPA receptors (GRIA). However, we assume there is successful compensatory

336   stabilization of actin filaments through the RhoA Signaling Pathway.

337   The RhoA Signaling Pathway represents only one of many pathways that were

338   found to be dysregulated in the pre-clinical 3m Tg-AD model. Understanding how these

339   pathways take part in the response to Aβ may lead to new therapeutic avenues for AD.

340   Additionally, recognition of the early dysregulation of these pathways may help identify

341   new, pre-clinical, phenotypes for AD.

Methods

Mice

344   Mice used in the experiments were housed in accordance with protocols approved

345   by the Institutional Animal Care and Use Committee at University of Colorado and all

346   experiments were conducted according to the NIH Guide for the Care and Use of

347   Laboratory Animals. The B6C3-Tg(APPswe, PSEN1dE9)85Dbo/J) breeding pair was

348   obtained from The Jackson Laboratory (stock number 004462). Colony was maintained

349   using +/+ sibling x Hemi zygote. Ear punches were taken at approximately 10 days old

350   and PCR identification was performed to identify AD transgenic mice and the non-

351   transgenic littermate controls. The AD transgenic mice and the non-transgenic littermate

352   controls of the same sex were housed in individual ventilated cages, with a maximum of

353   five mice per cage. Female B6C3-Tg(APPswe, PSEN1dE9)85Dbo/J) transgenic mice at

354   various ages (3, 5, and 9 months) and their age-matched, non-transgenic littermate

355   controls (wild type, WT) were used in this study. For quality control purposes tail clips

356   were taken at the time of death and a second genotyping was performed to confirm the

357   first.

ELISA

359   Hemi-brain samples were analyzed for human Aβ 1-40 and 1-42 using

360   commercially available ELISA kits (Life Technologies: KHB3481 & KHB3441) according

16

361   to manufacturer's instruction. Amounts of Aβ were normalized to total protein as

362   determined by BCA assay (Pierce #23225).

Synaptosome Isolation

364   All mice were sacrificed at the age indicated. Synaptosomes were isolated as

365   previously described with minor modifications (16). The whole brain was dissected from

366   one mouse and homogenized with 20 strokes in 2 mL of complete sucrose buffer (0.32

367   M Sucrose; 2 mM EGTA; 2 mM EDTA; 10 mM HEPES (pH 7.4), 1x Protease Inhibitor

368   Cocktail: cOmplete, EDTA-free (Roche 05 056 489 001), 1mM Na_3VO_4 (Sodium

369   Vanadate), 1mM $Na_4O_7P_2$ (Sodium Pyrophosphate). Centrifuged at 800 x g for 10 minutes

370   at 4°C to pellet the membrane fragments and nuclei and collect supernatant (S1) in 15

371   mL conical tubes then fast frozen in liquid nitrogen and then stored at 70°C until all mouse

372   brain samples for were collected. To minimize technical variability, synaptosomal

373   preparation was performed in age-matched batches. All batch purifications were

374   performed with the same stock buffers within 24 hours of each other. To prepare purified

375   synaptosomes the S1 samples were thawed on ice, centrifuged at 800 x g for 10 minutes

376   at 4°C and collect supernatant (S1') in high-speed polycarbonate tubes. S1' fractions

377   were then centrifuged at 10,000 x g for 15 minutes at 4°C to obtain a pellet (P2) containing

378   synaptosomes contaminated with mitochondria and microsomes. P2 was suspended in

379   500 μl of Complete Sucrose Buffer, vortexed thoroughly then loaded on a sucrose

380   gradient (from bottom to top): 1.18 M – 1.0 M – 0.85 M (all prepared in 10 mM HEPES,

381   pH 7.4, 2 mM EDTA, 2 mM EGTA) prior to centrifuging at 82,500 x g for 1 hour at 4°C.

382   Pure synaptosomes were collected from the interface between 1.0 M and 1.18 M, washed

383   by adding ~3X volume of Complete Sucrose Buffer and centrifuged at 10,000 x g for 15

17

384   minutes at 4°C prior to re-suspending in Complete Sucrose Buffer and measuring of

385   protein concentration using a micro BCA Protein Assay (Pierce 22660) according to

386   manufacturer's instructions. Pure synaptosomes were divided into 50 µg aliquots and

387   stored at -80°C.

Peptide Preparation

389   Peptide preparation was performed by the Filter Assisted Sample Preparation

390   (FASP) method as described (17). Briefly, to extract membrane proteins in the

391   synaptosome samples, a 0.3% concentration of Triton X-100 was used to solubilize 50

392   µg of purified synaptosomes. The sample was then washed with fresh 8 M and 2 M Urea

393   Buffer in a 30 kDa filter (Millipore UFC 503024); the proteins were reduced (10 mM TCEP)

394   and alkylated (25 mM IA) and treated with trypsin (Promega #V5113; 1:100 or 0.05 µg of

395   trypsin per 50 µg sample) overnight in the spin filter. The resulting peptides were desalted

396   in C-18 spin columns (Pierce 89870) according to the manufacturer's instructions. The

397   peptide concentration was estimated using a NanoDrop 2000 and Bovine Serum Albumin

398   as reference (mass extinction coefficient of 6.7 at 280 nm) resulting in 6-7 µg of peptide

399   per sample. The peptide was then immediately lyophilized for 2 hours, and stored at -

400   80°C.

RP-RP MS/MS

402   The peptides were separated by liquid chromatography using a nanoAcquity UPLC

403   system (Waters) coupled to a LTQ Orbitrap mass spectrometer (Thermo Fisher

404   Scientific). Peptide mixtures (2 µg) were loaded onto a 300-µm × 50-mm XBridge C18,

405   130-Å, 5-µm column maintained at pH 10.0, eluting peptides in six fractions

18

406   corresponding to 10%, 15%, 20%, 30%, 40%, and 60% buffer B1 (buffer A1: 20 mM

407   ammonium formate, pH 10.0; and buffer B1: 100% acetonitrile). Steps were eluted from

408   the high pH column at 20 µl/min onto a 180-µm × 20-mm C18, 100-Å, 5-µm trap column,

409   which was then switched in-line with the analytical column and eluted as in the 1D

410   method. For 1D analysis, a BEH C18 reversed phase column (25 cm × 75 µm i.d., 1.7

411   µm, 100 Å; Waters) was used for the analytical separation using a linear gradient from

412   90% buffer A2 (0.1% formic acid) to 40% buffer B2 (0.1% formic acid and 80%

413   acetonitrile) over 60 min at a flow rate of 300 nL/min.

414   MS/MS data were collected by an enabling monoisotopic precursor and charge

415   selection settings. Ions with unassigned charge state were excluded. For each mass

416   spectrometry scan, the 10 most intense ions were targeted with dynamic exclusion 30 s,

417   1 D exclusion width, and repeat count equal to 1. The maximum injection time for Orbitrap

418   parent scans was 500 ms, allowing 1 microscan and automatic gain control of 106. The

419   maximal injection time for the LTQ MS/MS was 250 ms, with 1 microscan and automatic

420   gain control of 104. The normalized collision energy was 35%, with activation Q of 0.25

421   for 30 ms.

422   **Data Analysis**

423   The raw MS/MS data from all samples were analyzed by MaxQuant (37)(version

424   1.5.2.8). Andromeda (38), a probabilistic search engine incorporated into the MaxQuant

425   framework was used to search the peak list against the Uniprot_MOUSE database

426   (UniProtKB release 2016_098, entries: 82,200). Common contaminants were added to

427   this database. The search included cysteine carbamidomethylation as a fixed modification

428   and N-terminal acetylation and methionine oxidation as variable modifications. The false

429   discovery rate (FDR) was set to 0.01 for both peptide and protein identifications. Enzyme

430   specificity was set to trypsin allowing N-terminal cleavage to proline. Two miscleavages

431   were allowed, and a minimum of seven amino acids per identified peptide were required.

432   Peptide identification was based on a search with an initial mass deviation of the

433   precursor ion (ITMS) of up to 0.5 Da, and the allowed fragment mass deviation (FTMS)

434   was set to 20 ppm. Razor peptides were used for quantification; unmodified or with the

435   modifications specified above. To match identifications across different replicates and

436   adjacent fractions, the "match between runs" option in MaxQuant was enabled within a

437   matching time window of 0.7 min.

438   Bioinformatics analysis was done with Perseus (39)(version 1.4.1.3) tools

439   available in the MaxQuant environment. The proteins only identified by site, from the

440   reverse database, and contaminant proteins were removed from the matrix. Categorical

441   annotation by age and type was performed resulting in 6 groups: AD_3M, AD_5M,

442   AD_9M, WT_3M, WT_5M, & WT_9M, with an n=3 in each group. The protein matrix was

443   reduced to those identifications with at least one valid observation in each group. A

444   multiple-sample test was run between WT_3M, WT_5M, & WT_9M using a Bengamini-

445   Hochburg FDR=0.25 (7 significant) and these proteins were removed from the matrix.

446   The 9 WT samples were then pooled into one WT group and the data was exported for

447   further analysis with R version 3.3.1 (2016-06-21) and the package limma (21,23) (version

448   3.28.14). Limma was then used to calculate the $\log_2$ fold change and the empirical Bayes

449   p-Value between the following groups: AD_9m & WT, AD_5m & WT, AD_3m & WT,

450   WT_9m & WT, WT_5m & WT, and WT_3m & WT.

451 # Acknowledgements

452

453 # References

454 1. Purves D, Augustine GJ, Fitzpatrick D, Hall WC, LaMantia A-S, McNamara JO, et al.,
455   editors. Neuroscience. 3rd ed. Sunderland, MA: Sinaur Associates, Inc; 2004. 832 p.

456 2. Boyd-Kimball D, Castegna A, Sultana R, Poon HF, Petroze R, Lynn BC, et al. Proteomic
457   identification of proteins oxidized by Abeta(1-42) in synaptosomes: implications for
458   Alzheimer's disease. Brain Res. 2005 May 24;1044(2):206–15.

459 3. Schrimpf SP, Meskenaite V, Brunner E, Rutishauser D, Walther P, Eng J, et al. Proteomic
460   analysis of synaptosomes using isotope-coded affinity tags and mass spectrometry.
461   PROTEOMICS. 2005;5(10):2531–2541.

462 4. Witzmann FA, Arnold RJ, Bai F, Hrncirova P, Kimpel MW, Mechref YS, et al. A proteomic
463   survey of rat cerebral cortical synaptosomes. Proteomics. 2005 May;5(8):2177–201.

464 5. Bai F, Witzmann FA. Synaptosome proteomics. Subcell Biochem. 2007;43:77–98.

465 6. Siu SO, Lam MPY, Lau E, Kong RPW, Lee SMY, Chu IK. Fully automatable two-
466   dimensional reversed-phase capillary liquid chromatography with online tandem mass
467   spectrometry for shotgun proteomics. Proteomics. 2011 Jun;11(11):2308–19.

468 7. Walsh DM, Klyubin I, Fadeeva JV, Cullen WK, Anwyl R, Wolfe MS, et al. Naturally
469   secreted oligomers of amyloid β protein potently inhibit hippocampal long-term potentiation
470   in vivo. Nature. 2002 Apr 4;416(6880):535–9.

471 8. Harmeier A, Wozny C, Rost BR, Munter L-M, Hua H, Georgiev O, et al. Role of Amyloid-
472   β Glycine 33 in Oligomerization, Toxicity, and Neuronal Plasticity. J Neurosci. 2009 Jun
473   10;29(23):7582–90.

474 9. Terry RD, Masliah E, Salmon DP, Butters N, DeTeresa R, Hill R, et al. Physical basis of
475   cognitive alterations in Alzheimer's disease: synapse loss is the major correlate of cognitive
476   impairment. Ann Neurol. 1991 Oct;30(4):572–80.

477 10. Kim SI, Voshol H, van Oostrum J, Hastings TG, Cascio M, Glucksman MJ.
478   Neuroproteomics: expression profiling of the brain's proteomes in health and disease.
479   Neurochem Res. 2004 Jun;29(6):1317–31.

480 11. Reiserer RS, Harrison FE, Syverud DC, McDonald MP. Impaired spatial learning in the
481   APPSwe + PSEN1DeltaE9 bigenic mouse model of Alzheimer's disease. Genes Brain Behav.
482   2007 Feb;6(1):54–65.
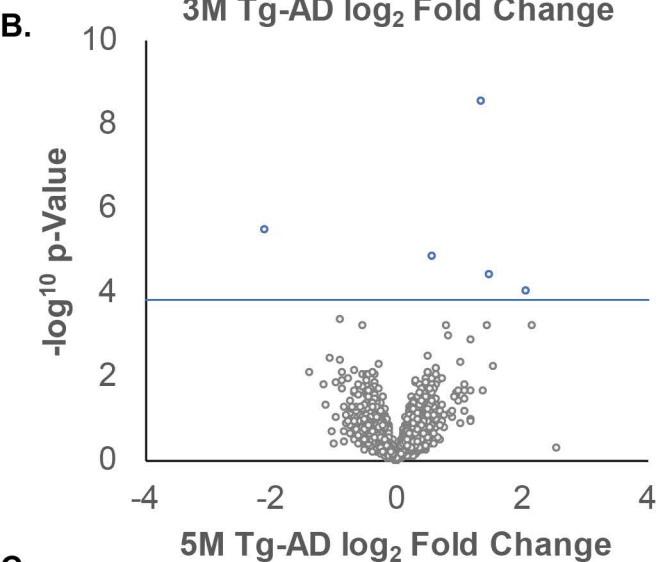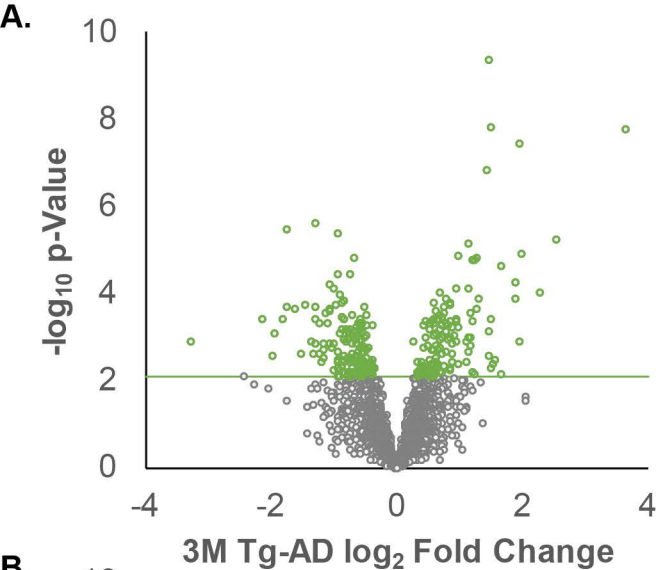
483   12.   Spires TL, Hyman BT. Transgenic models of Alzheimer's disease: learning from animals.
484   NeuroRx J Am Soc Exp Neurother. 2005 Jul;2(3):423–37.

485   13.   Harrison FE, Hosseini AH, McDonald MP, May JM. Vitamin C reduces spatial learning
486   deficits in middle-aged and very old APP/PSEN1 transgenic and wild-type mice. Pharmacol
487   Biochem Behav. 2009 Oct;93(4):443–50.

488   14.   Garcia-Alloza M, Robbins EM, Zhang-Nunes SX, Purcell SM, Betensky RA, Raju S, et al.
489   Characterization of amyloid deposition in the APPswe/PS1dE9 mouse model of Alzheimer
490   disease. Neurobiol Dis. 2006 Dec;24(3):516–24.

491   15.   Takeda S, Hashimoto T, Roe AD, Hori Y, Spires-Jones TL, Hyman BT. Brain interstitial
492   oligomeric amyloid β increases with age and is resistant to clearance from brain in a mouse
493   model of Alzheimer's disease. FASEB J Off Publ Fed Am Soc Exp Biol. 2013
494   Aug;27(8):3239–48.

495   16.   Hajós F. An improved method for the preparation of synaptosomal fractions in high purity.
496   Brain Res. 1975 Aug 15;93(3):485–9.

497   17.   Wiśniewski JR, Zougman A, Nagaraj N, Mann M. Universal sample preparation method for
498   proteome analysis. Nat Methods. 2009 May;6(5):359–62.

499   18.   Tyanova S, Temu T, Carlson A, Sinitcyn P, Mann M, Cox J. Visualization of LC-MS/MS
500   proteomics data in MaxQuant. PROTEOMICS. 2015 Apr 1;15(8):1453–6.

501   19.   Cox J, Hein MY, Luber CA, Paron I, Nagaraj N, Mann M. Accurate Proteome-wide Label-
502   free Quantification by Delayed Normalization and Maximal Peptide Ratio Extraction,
503   Termed MaxLFQ. Mol Cell Proteomics MCP. 2014 Sep;13(9):2513–26.

504   20.   Schaab C, Geiger T, Stoehr G, Cox J, Mann M. Analysis of High Accuracy, Quantitative
505   Proteomics Data in the MaxQB Database. Mol Cell Proteomics MCP [Internet]. 2012 Mar
506   [cited   2015   Nov   6];11(3).   Available   from:
507   http://www.ncbi.nlm.nih.gov/pmc/articles/PMC3316731/

508   21.   Ritchie ME, Phipson B, Wu D, Hu Y, Law CW, Shi W, et al. limma powers differential
509   expression analyses for RNA-sequencing and microarray studies. Nucleic Acids Res. 2015
510   Apr 20;43(7):e47.

511   22.   Phipson B, Lee S, Majewski IJ, Alexander WS, Smyth GK. Robust hyperparameter
512   estimation protects against hypervariable genes and improves power to detect differential
513   expression. Ann Appl Stat. 2016 Jun;10(2):946–63.

514   23.   Smyth GK. Linear models and empirical bayes methods for assessing differential expression
515   in microarray experiments. Stat Appl Genet Mol Biol. 2004;3:Article3.

516   24.   Campion D, Pottier C, Nicolas G, Le Guennec K, Rovelet-Lecrux A. Alzheimer disease:
517   modeling an Aβ-centered biological network. Mol Psychiatry. 2016 Jul;21(7):861–71.

25. Ernst J, Bar-Joseph Z. STEM: a tool for the analysis of short time series gene expression data. BMC Bioinformatics. 2006 Apr 5;7:191.

26. Sevigny J, Chiao P, Bussière T, Weinreb PH, Williams L, Maier M, et al. The antibody aducanumab reduces Aβ plaques in Alzheimer's disease. Nature. 2016 Sep 1;537(7618):50–6.

27. Morgan CD, Murphy C. Individuals at risk for Alzheimer's disease show differential patterns of ERP brain activation during odor identification. Behav Brain Funct. 2012 Jul 31;8(1):37.

28. Attems J, Walker L, Jellinger KA. Olfactory bulb involvement in neurodegenerative diseases. Acta Neuropathol (Berl). 2014 Apr;127(4):459–75.

29. Alberdi E, Sánchez-Gómez MV, Cavaliere F, Pérez-Samartín A, Zugaza JL, Trullas R, et al. Amyloid beta oligomers induce Ca2+ dysregulation and neuronal death through activation of ionotropic glutamate receptors. Cell Calcium. 2010 Mar;47(3):264–72.

30. Bieschke J, Herbst M, Wiglenda T, Friedrich RP, Boeddrich A, Schiele F, et al. Small-molecule conversion of toxic oligomers to nontoxic β-sheet-rich amyloid fibrils. Nat Chem Biol. 2011 Nov 20;8(1):93–101.

31. Shelat PB, Chalimoniuk M, Wang J-H, Strosznajder JB, Lee JC, Sun AY, et al. Amyloid beta peptide and NMDA induce ROS from NADPH oxidase and AA release from cytosolic phospholipase A2 in cortical neurons. J Neurochem. 2008 Jul 1;106(1):45–55.

32. Mattson MP, Cheng B, Davis D, Bryant K, Lieberburg I, Rydel RE. beta-Amyloid peptides destabilize calcium homeostasis and render human cortical neurons vulnerable to excitotoxicity. J Neurosci Off J Soc Neurosci. 1992 Feb;12(2):376–89.

33. Mendoza-Naranjo A, Contreras-Vallejos E, Henriquez DR, Otth C, Bamburg JR, Maccioni RB, et al. Fibrillar amyloid-β1-42 modifies actin organization affecting the cofilin phosphorylation state: a role for Rac1/cdc42 effector proteins and the slingshot phosphatase. J Alzheimers Dis JAD. 2012;29(1):63–77.

34. Woo JA, Boggess T, Uhlar C, Wang X, Khan H, Cappos G, et al. RanBP9 at the intersection between cofilin and Aβ pathologies: rescue of neurodegenerative changes by RanBP9 reduction. Cell Death Dis. 2015 Mar 5;6:1676.

35. Yuen EY, Yan Z. Dopamine D4 Receptors Regulate AMPA Receptor Trafficking and Glutamatergic Transmission in GABAergic Interneurons of Prefrontal Cortex. J Neurosci Off J Soc Neurosci. 2009 Jan 14;29(2):550–62.

36. Correia SS, Bassani S, Brown TC, Lisé M-F, Backos DS, El-Husseini A, et al. Motor protein–dependent transport of AMPA receptors into spines during long-term potentiation. Nat Neurosci. 2008 Apr;11(4):457–66.

552   37.   Cox J, Mann M. MaxQuant enables high peptide identification rates, individualized p.p.b.-
553   range mass accuracies and proteome-wide protein quantification. Nat Biotechnol. 2008
554   Dec;26(12):1367–72.

555   38.   Cox J, Neuhauser N, Michalski A, Scheltema RA, Olsen JV, Mann M. Andromeda: A Peptide
556   Search Engine Integrated into the MaxQuant Environment. J Proteome Res. 2011 Apr
557   1;10(4):1794–805.

558   39.   Cox J, Mann M. 1D and 2D annotation enrichment: a statistical method integrating
559   quantitative proteomics with complementary high-throughput data. BMC Bioinformatics.
560   2012;13 Suppl 16:S12.

561

A.

B.

3M
- Low Aβ load
- Pre-Aβ plaque
- No Cognitive Decline

5M
- Medium-high Aβ load
- Sporadic Aβ plaque
- No Cognitive Decline

9M
- High Aβ load
- Characteristic Aβ plaque
- Mild Cognitive Decline

A.

B.

C.

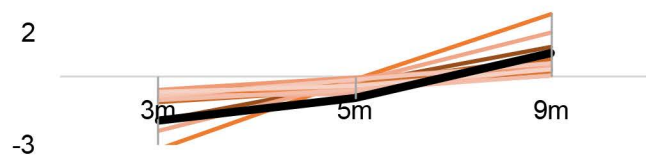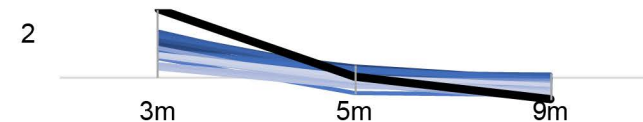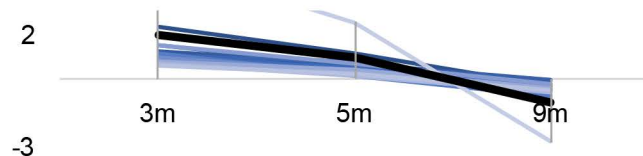**A.** (-3, 0, 1)
P-Value = 3E-15

B. (-1, 0, 3)
P-Value = 2E-06
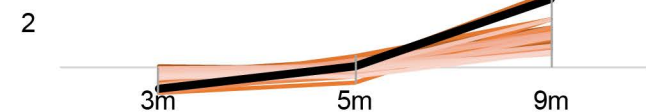
C. (-2, -1, 1)
P-Value = 2E-05

D. (3, 0, -1)
P-Value = 3E-05

E. (2, 1, -1)
P-Value = 3E-04

Canonical Pathway	p-Value			z-Score		
	3m (FDR=0.1 FC=1)	3m (FDR = 0.1)	3m (FDR = 0.1, FC >= 0.4, +STEM)	3m (FDR=0.1 FC=1)	3m (FDR = 0.1)	3m (FDR = 0.1, FC >= 0.4, +STEM)
EIF2 Signaling	1.5	0.5	1.3	N/A	N/A	2.2
Phospholipase C Signaling	0.0	1.9	2.3	0.0	1.0	1.9
RhoA Signaling	0.0	2.3	2.3	0.0	1.6	1.9
Actin Cytoskeleton Signaling	0.3	2.6	2.4	N/A	1.0	1.2
Endothelin-1 Signaling	0.9	1.1	1.3	N/A	0.4	0.7
Signaling by Rho Family GTPases	0.3	2.9	2.6	N/A	0.7	0.6
PPARα/RXRα Activation	0.0	0.4	2.3	0.0	N/A	-1.7
Glutamate Receptor Signaling	1.9	4.1	3.7	N/A	-0.4	-0.4
Mitochondrial Dysfunction	4.8	6.6	7.6	N/A	N/A	N/A
Oxidative Phosphorylation	3.4	5.0	5.5	N/A	N/A	N/A

p-Value Color Key: 0 2 4 6 8 10

z-Score Color Key: -2.0 -1.0 -0.5 0.0 0.5 1.0 2.0

Canonical Pathway	STEM enriched		
	3m	5m	9m
RhoA Signaling	1.9	0.8	N/A
Phospholipase C Signaling	1.9	2.4	1.3
Actin Cytoskeleton Signaling	1.2	0.3	1.7
EIF2 Signaling	2.2	1.3	-1.3
α-Adrenergic Signaling	0.8	1.6	-0.4
Thrombin Signaling	0.4	1.1	-0.4
Signaling by Rho Family GTPases	0.6	-0.3	1.6
CREB Signaling in Neurons	0.7	-0.7	1.1
NRF2-mediated Oxidative Stress Response	1.3	-0.4	0.4
IL-1 Signaling	1.0	-1.0	N/A
Synaptic Long Term Potentiation	0.8	-0.4	-0.4
Synaptic Long Term Depression	0.4	-1.1	-1.3
G Beta Gamma Signaling	1.3	-0.4	-1.0
Huntington's Disease Signaling	1.0	0.0	-1.0
Endothelin-1 Signaling	0.7	0.0	-1.3
fMLP Signaling in Neutrophils	1.0	N/A	N/A
Ephrin Receptor Signaling	0.8	0.0	0.0
Fcγ Receptor-mediated Phagocytosis in Macrophages and Monocytes	0.4	N/A	N/A
Integrin Signaling	-0.3	0.8	1.1
Calcium Signaling	0.0	0.4	1.6
Insulin Receptor Signaling	-0.4	1.1	-0.4
RhoGDI Signaling	-0.7	0.4	N/A
PPARα/RXRα Activation	-1.7	-1.0	2.1
Glutamate Receptor Signaling	-0.4	-1.3	1.0
Apoptosis Signaling	-1.0	-1.0	1.0
LPS/IL-1 Mediated Inhibition of RXR Function	0.0	N/A	-1.0
Gαi Signaling	-1.3	-0.4	-2.0

-2.0	-1.0	-0.5	0.0	0.5	1.0	2.0

z-Score Color Key
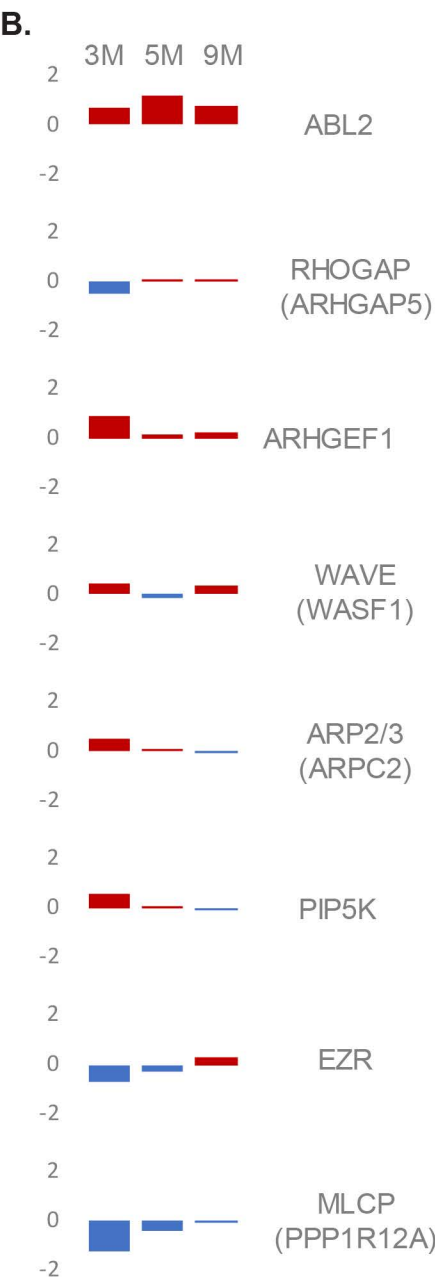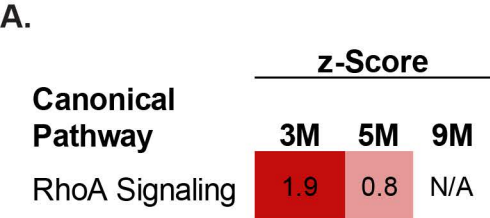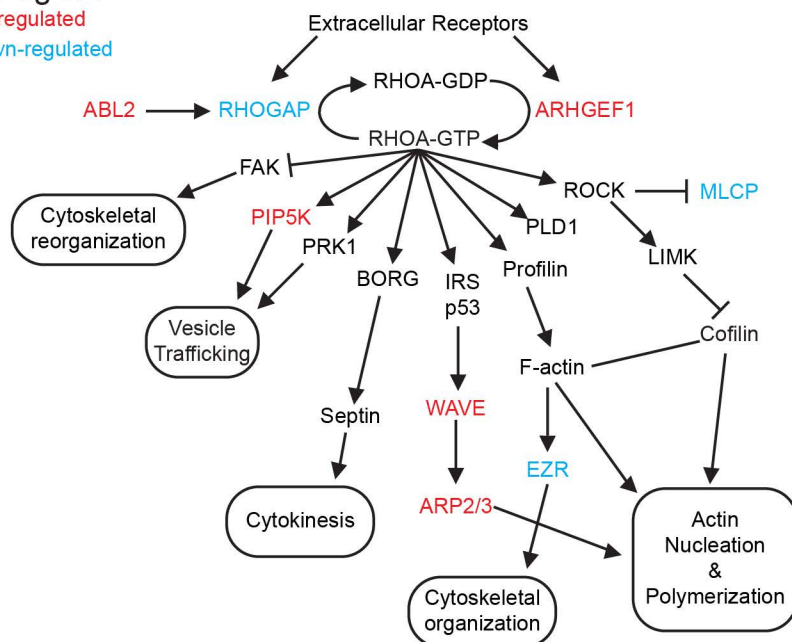
Aβ impact on Cofilin & Actin Stabilization

Activated
Inhibited
Inconsistent with state of downstream molecule